Reaction mechanism in odd-even staggering of reaction cross sections

Satoru Sasabe,[1,*] Takuma Matsumoto,[1] Shingo Tagami,[1] Naoya Furutachi,[2] Kosho Minomo,[1]
Yoshifumi R. Shimizu,[1] and Masanobu Yahiro[1]
[1]*Department of Physics, Kyushu University, Fukuoka 812-8581, Japan*
[2]*Department of Physics, Hokkaido University, Sapporo 060-0810, Japan*
(Received 13 May 2013; revised manuscript received 30 July 2013; published 18 September 2013)

It was recently suggested that the odd-even staggering of reaction cross sections is evidence of the pairing anti-halo effect on projectile radii. We define the dimensionless staggering parameters $\Gamma_{\rm rds}$ and $\Gamma_{\rm R}$ for projectile radii and reaction cross sections, respectively, and analyze the relation between $\Gamma_{\rm rds}$ and $\Gamma_{\rm R}$ for the scattering of ^{14,15,16}C from a ^{12}C target at 83 MeV/nucleon by taking account of projectile-breakup and nuclear-medium effects with the microscopic version of the continuum discretized coupled-channels method. The value of $\Gamma_{\rm R}$ deviates from that of $\Gamma_{\rm rds}$ by the projectile-breakup effect, the nuclear-medium effect, and an effect resulting from the fact that the scattering is not exactly black-sphere scattering (BSS). The projectile-breakup and nuclear medium effects nearly cancel for $\Gamma_{\rm R}$ at low incident energies. The remaining non-BSS effect becomes small as the incident energy decreases, indicating that nucleus-nucleus scattering at lower incident energies can be a good probe for evaluating $\Gamma_{\rm rds}$ from measured reaction cross sections.

DOI: 10.1103/PhysRevC.88.037602 PACS number(s): 24.10.Eq, 25.60.Gc, 25.60.Bx

Introduction. The interaction cross section $\sigma_{\rm I}$ and the reaction cross section $\sigma_{\rm R}$ are important tools for determining the radii of unstable nuclei. Actually, the halo structure as an exotic property has been reported for unstable nuclei such as ^{11}Li through analyses of measured $\sigma_{\rm I}$ values [1,2]. Very recently, $\sigma_{\rm I}$ was measured for Ne isotopes [3] and it is suggested by the analyses [4,5] that ^{31}Ne is a halo nucleus with large deformation.

The difference between $\sigma_{\rm I}$ and $\sigma_{\rm R}$ is considered to be small for scattering of unstable nuclei at intermediate energies [6]. The reaction cross section is related to the radius of the projectile; for example, see Ref. [6] for a detailed analyses. Meanwhile, it is well known that the pairing correlation is important, particularly in even-N nuclei. The correlation becomes essential in weakly bound nuclei, since they are not bound without it. The effects of the pairing correlation on nuclear radii of unstable nuclei were investigated by using the Hartree-Fock Bogoliubov (HFB) method [7]. In the mean-field picture, the correlation makes the quasiparticle energy larger and hence reduces the root-mean-square (rms) radius of the HFB density. Obviously, this effect is conspicuous for unstable nuclei with separation energy smaller than the gap energy. Thus, the pairing correlation suppresses the growth of the halo structure for even-even unstable nuclei. This is now called the pairing anti-halo effect.

The pairing anti-halo effect is an interesting phenomenon, but clear evidence has yet to be shown for the effect. Very recently, however, Hagino and Sagawa suggested that the observed odd-even staggerings of $\sigma_{\rm R}$ are possible evidence of the effect [8–10]. They introduced the staggering parameter [10]

$$\gamma_3 = -\frac{\sigma_{\rm R}(A_{\rm P}) - 2\sigma_{\rm R}(A_{\rm P}+1) + \sigma_{\rm R}(A_{\rm P}+2)}{2}, \qquad (1)$$

where the mass number $A_{\rm P}$ of the projectile is assumed to be even. In Ref. [8], the staggering was analyzed with the HFB method for ^{30,31,32}Ne + ^{12}C scattering at 240 MeV/nucleon [3] and with the three-body model for ^{14,15,16}C + ^{12}C scattering at 83 MeV/nucleon [11]. The analyses are successful in reproducing the observed staggerings [3,11], although the reaction calculations are based on the Glauber model.

In this Brief Report, we reanalyze ^{14,15,16}C scattering in order to focus our attention on the reaction mechanism, since ^{15}C has a simpler structure than ^{31}Ne in the sense that the energy of the first excited state in ^{14}C as a core nucleus is much larger than that in ^{30}Ne. For ^{14,15,16}C, γ_3 is 163 ± 52 mb, which is about 10% of $\sigma_{\rm R}(^{15}{\rm C}) = 1319 \pm 40$ mb [11]. Thus the pairing anti-halo effect may be comparable with the projectile-breakup and nuclear-medium effects, which are not taken into account in the previous analysis. Therefore, we investigate these effects on the staggering, using the continuum-discretized coupled-channels method (CDCC) [12–14]. CDCC for two-body (three-body) projectiles is often called three-body (four-body) CDCC; in the naming the target degree of freedom is taken into account. Here we apply four-body CDCC to ^{16}C.

Theoretical framework. Following Ref. [8], we assume the $n + {}^{14}$C two-body model for ^{15}C and the $n + n + {}^{14}$C three-body model for ^{16}C. The three-body model of ^{16}C is a simple model for treating the pairing correlation between two extra neutrons. In the present calculation, breakup processes of ^{15}C and ^{16}C on ^{12}C are described by the $n + {}^{14}{\rm C} + {}^{12}$C three-body model and the $n + n + {}^{14}{\rm C} + {}^{12}$C four-body model, respectively. The Schrödinger equation is defined as

$$(H - E)\Psi = 0 \qquad (2)$$

for the total wave function Ψ, where E is the energy of the total system. The total Hamiltonian H is defined by

$$H = K_R + U + h, \qquad (3)$$

where h denotes the internal Hamiltonian of ^{15}C or ^{16}C and $\boldsymbol{R}$ is the center-of-mass coordinate of the projectile relative to a ^{12}C

*sasabe@email.phys.kyushu-u.ac.jp

target. The kinetic energy operator associated with $\boldsymbol{R}$ is represented by K_R, and U is the sum of interactions between the constituents in the projectile (P) and the target (T) defined as

$$U = U_n(R_n) + U_{^{14}\mathrm{C}}(R_{^{14}\mathrm{C}}) + \frac{e^2 Z_\mathrm{P} Z_\mathrm{T}}{R} \tag{4}$$

for ^{15}C and

$$U = U_{n_1}(R_{n_1}) + U_{n_2}(R_{n_2}) + U_{^{14}\mathrm{C}}(R_{^{14}\mathrm{C}}) + \frac{e^2 Z_\mathrm{P} Z_\mathrm{T}}{R} \tag{5}$$

for ^{16}C, where U_x $(x = n, n_1, n_2, ^{14}\mathrm{C})$ is the nuclear part of the optical potential between x and ^{12}C as a function of the relative coordinate R_x.

The optical potential U_x is constructed microscopically by folding the Melbourne g-matrix nucleon-nucleon interaction [15] with densities of x and ^{12}C. For ^{12}C, the proton density is obtained phenomenologically from the electron scattering [16], and the neutron density is assumed to be the same as the proton one, since the proton rms radius deviates from the neutron one only by less than 1% in the HFB calculation. For ^{14}C, the matter density is determined by the HFB calculation with the Gogny-D1S interaction [17], where the center-of-mass correction is made in the standard manner [6]. As shown latter, the total reaction cross section calculated with the folding potential $U_{^{14}\mathrm{C}}$ yields good agreement with the experimental data for $^{14}\mathrm{C} + ^{12}\mathrm{C}$ scattering at 83 MeV/nucleon. The Melbourne g-matrix folding method is successful in reproducing nucleon-nucleus and nucleus-nucleus elastic scattering systematically [6,14]. The folding potentials thus obtained include *the nuclear-medium effect*. CDCC with these microscopic potentials is the microscopic version of CDCC.

In the present system, Coulomb breakup is quite small, since the projectile and the target are light nuclei, and hence the Coulomb barrier energy between P and T is much smaller than the incident energy considered here. We then neglect Coulomb breakup, as shown in Eq. (5), where Z_P and Z_T are the atomic numbers of nuclei P and T, respectively.

For ^{15}C, we take the n-^{14}C interaction of Ref. [8], which well reproduces properties of the ground and first-excited states of ^{15}C. For ^{16}C, we use the Bonn-A interaction [18] between two neutrons, the same interaction as in Ref. [8] between n and ^{14}C, and introduce a total-spin-dependent three-body interaction to reproduce energies of the ground 0^+ state and the first 2^+ excited state of ^{16}C. Eigenstates of h are obtained with the numerical techniques of Ref. [19]; that is, the orthogonality condition is imposed. Now we introduce the dimensionless staggering parameter Γ_rds for the projectile and target rms radii $\bar{r}(A_\mathrm{P})$ and $\bar{r}(A_\mathrm{T})$:

$$\Gamma_\mathrm{rds} = \frac{\bar{R}^2(A_\mathrm{P}+1) - [\bar{R}^2(A_\mathrm{P}) + \bar{R}^2(A_\mathrm{P}+2)]/2}{[\bar{R}^2(A_\mathrm{P}+2) - \bar{R}^2(A_\mathrm{P})]/2} \tag{6}$$

with

$$\bar{R}(A_\mathrm{P}) = \bar{r}(A_\mathrm{P}) + \bar{r}(A_\mathrm{T}). \tag{7}$$

Note that $\Gamma_\mathrm{rds} \geqslant 1$ when $\bar{r}(A_\mathrm{P}+1) \geqslant \bar{r}(A_\mathrm{P}+2)$. The matter radii of ^{14,15,16}C are summarized in Table I. The present two-body and three-body models yield $\Gamma_\mathrm{rds} = 1.3$ for ^{14,15,16}C.

TABLE I. Matter radii of ^{14,15,16}C.

	$\bar{r}(^{14}\mathrm{C})$ (fm)	$\bar{r}(^{15}\mathrm{C})$ (fm)	$\bar{r}(^{16}\mathrm{C})$ (fm)
Calc.	2.51[a]	2.87[a]	2.83[a]
	2.53[b]	2.90[b]	2.81[b]
Exp.	2.50[c]	–	–

[a]Present calculation.
[b]Reference [8].
[c]Charge radius [20].

In the CDCC method, eigenstates of h consist of a finite number of discrete states with negative energies and discretized continuum states with positive energies. The Schrödinger equation (2) is solved in a model space $\mathcal{P}$ spanned by the discrete and discretized continuum states:

$$\mathcal{P}(H - E)\mathcal{P}\Psi_\mathrm{CDCC} = 0. \tag{8}$$

Following Ref. [21], we obtain the discrete and discretized continuum states by diagonalizing h in a space spanned by the Gaussian basis functions. The elastic and discrete breakup S-matrix elements are obtained by solving the CDCC equation (8) under the standard asymptotic boundary condition [12,23]. In actual calculations, we neglect the projectile spin, since the effect is small on σ_R [6,24]. Breakup states are taken up to the g wave for ^{15}C. Meanwhile, only 0^+ and 2^+ breakup states are considered for ^{16}C, because the effect of 1^- breakup states on σ_R is found to be less than 1%. In all the present calculations, we have confirmed convergence of the CDCC solution for σ_R.

Now we define the dimensionless staggering parameter also for σ_R:

$$\Gamma_\mathrm{R} = \frac{\gamma_3}{[\sigma_\mathrm{R}(A_\mathrm{P}+2) - \sigma_\mathrm{R}(A_\mathrm{P})]/2}, \tag{9}$$

where $\Gamma_\mathrm{R} = 0$ when $\sigma_\mathrm{R}(A_\mathrm{P}+1) = [\sigma_\mathrm{R}(A_\mathrm{P}+2) + \sigma_\mathrm{R}(A_\mathrm{P})]/2$ and $\Gamma_\mathrm{R} \geqslant 1$ when $\sigma_\mathrm{R}(A_\mathrm{P}+1) \geqslant \sigma_\mathrm{R}(A_\mathrm{P}+2)$. When the absolute value of the elastic S-matrix element, $|S_\mathrm{el}(L)|$, is 0 for orbital angular momenta L corresponding to the nuclear interior and 1 for those to the nuclear exterior, the following relationship is satisfied: $\sigma_\mathrm{R}(A_\mathrm{P}) \propto \bar{R}^2(A_\mathrm{P})$ [24]. In black-sphere scattering (BSS), Eq. (9) is reduced to $\Gamma_\mathrm{R} = \Gamma_\mathrm{rds}$. Once this condition is satisfied, Γ_R does not depend on the incident energy E_in. The staggering parameter can be evaluated from the measured σ_R for $^{14-16}\mathrm{C} + ^{12}\mathrm{C}$ scattering at 83 MeV/nucleon. The resulting value $\Gamma_\mathrm{R}^\mathrm{exp} = 2.0 \pm 0.8$ is consistent with $\Gamma_\mathrm{rds} = 1.3$. Three types of models are considered to investigate the nuclear-medium and projectile-breakup effects on σ_R.

Model I is the T-matrix folding model that has no nuclear-medium and projectile-breakup effects. The U_x are constructed from the Melbourne g-matrix nucleon-nucleon interaction at zero density. The single-channel calculation is done in (8).

Model II is the g-matrix folding model that has the nuclear-medium effect but not the projectile-breakup effect. This is the same as Model I, but the density dependence of the Melbourne g matrix is properly taken.

Model III is the model that has both the nuclear-medium and the projectile-breakup effects. CDCC calculations are done for

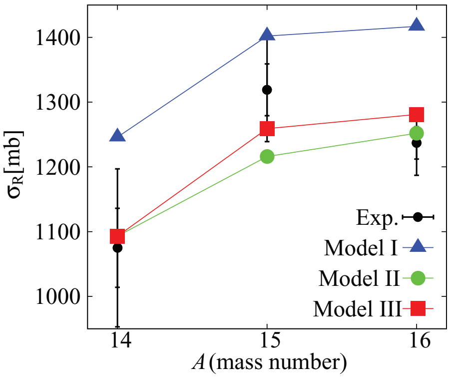

FIG. 1. (Color online) Reaction cross sections σ_R for ^{14,15,16}C + ^{12}C scattering at 83 MeV/nucleon. Triangle, circle, and square symbols stand for results of Models I, II, and III, respectively. The experimental data are taken from Ref. [11].

^{15,16}C scattering, but the g-matrix folding model is taken for ^{14}C scattering, since ^{14}C is a tightly bound system.

Results. Figure 1 shows σ_R for $^{14,15,16}\text{C} + {}^{12}\text{C}$ scattering at 83 MeV/nucleon. Triangle, circle, and square symbols stand for the results of Models I, II, and III, respectively. Model III well reproduces the experimental data [11], whereas Model I largely overestimates them; here the data are plotted with 2σ error (95.4% certainty). The net effect of nuclear-medium and projectile-breakup effects is thus important for σ_R. Model III yields $\Gamma_R = 0.77$, which deviates from $\Gamma_{\rm rds} = 1.3$. When the breakup effect is switched off from Model III, σ_R is reduced from squares to circles. This reduction is most significant for ^{15}C, so that Γ_R is reduced from 0.77 to 0.55. Furthermore, when the medium effect is switched off from Model II, the σ_R values are enhanced by about 10% from circles to triangles for all the cases of ^{14,15,16}C. More precisely, the enhancement is 13% for ^{14,16}C but 15% for ^{15}C, and, consequently, Γ_R increases from 0.55 to 0.82 by neglecting the medium effect. Thus the breakup and medium effects nearly cancel each other for Γ_R. The resultant value $\Gamma_R = 0.82$ is still considerably deviated from $\Gamma_{\rm rds} = 1.3$. This means that the present scattering is not BSS exactly. This remaining effect, i.e., the difference between $\Gamma_{\rm rds}$ and Γ_R of Model I, is referred to as the "non-BSS effect" in this Brief Report and is explicitly investigated below.

In the g-matrix folding model, the imaginary part of the folding potential, is often renormalized to reproduce the experimental data; see, for example, Ref. [22]. Our results of Models II and III are consistent with the measured σ_R without introducing such a renormalization, since we use the Melbourne g-matrix interaction. A 20% increase of the imaginary part of the folding potential enhances σ_R by about 6% for all of ^{14,15,16}C. Thus Γ_R is not sensitive to the magnitude of the imaginary part.

Figure 2 shows the absorption probability $P(L) \equiv 1 - |S_{\rm el}(L)|^2$ and the partial reaction cross section $\sigma_R(L) \equiv (2L+1)P(L)\pi/K^2$ as a function of L, where $\hbar K$ is an initial momentum of the elastic scattering. Here Model I is taken. For all the ^{14,15,16}C scattering, $P(L)$ behaves as not a step function but a logistic function. Thus the scattering are not the BSS exactly. Furthermore, L dependencies of the $P(L)$ are different among the three projectiles at $60 \lesssim L \lesssim 150$ corresponding to

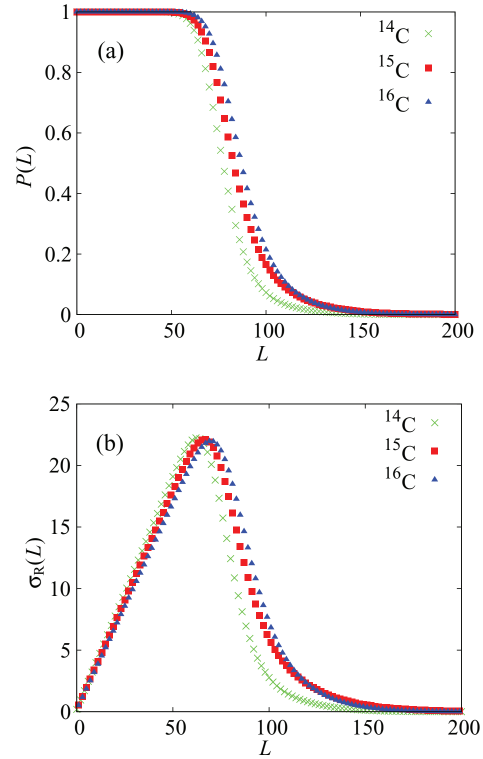

FIG. 2. (Color online) L dependence of (a) the absorption probability $P(L)$ and (b) the partial reaction cross section for ^{14,15,16}C + ^{12}C scattering at 83 MeV/nucleon. Model I is taken.

the peripheral region of a ^{12}C target. As a consequence of the difference, σ_R is not proportional to $\bar{R}^2$ properly. In fact, ^{15}C has a larger rms radius than ^{16}C, but ^{15}C scattering has a smaller $\sigma_R(L)$ than ^{16}C one at $70 \lesssim L \lesssim 120$ because of the fact that the volume integral of the imaginary part of the folding potential $\langle\varphi_0|U|\varphi_0\rangle$ is smaller for ^{15}C projectile than for ^{16}C projectile; here φ_0 is the projectile ground-state wave function.

Figure 3 shows the $E_{\rm in}$ dependence of Γ_R. Triangle, circle, and square symbols correspond to the results of Models I, II, and III, respectively, whereas the solid straight line denotes $\Gamma_{\rm rds}$. The deviation of triangles from the solid straight line shows the non-BSS effect, the deviation of circles from

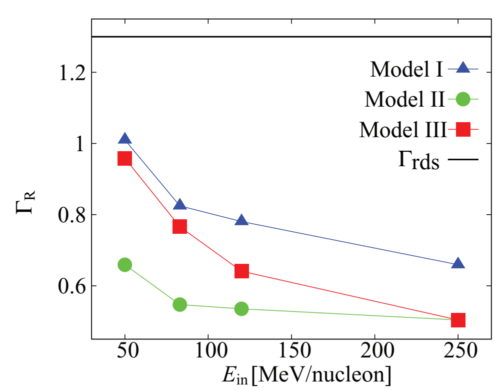

FIG. 3. (Color online) $E_{\rm in}$ dependence of Γ_R. Triangle, circle, and square symbols stand for the results of Models I, II, and III, respectively. The solid straight line denotes $\Gamma_{\rm rds}$.

triangles shows the nuclear-medium effect, and the deviation of squares from circles comes from the projectile-breakup effect. As E_{in} increases, the breakup effect decreases rapidly, but the non-BSS effect increases. The nuclear-medium effect also decreases but very slowly. Thus the non-BSS and medium effects are important for Γ_{R} at higher E_{in} around 250 MeV/nucleon, where the breakup has a less than 1% effect on σ_{R}. At lower E_{in} from 50 to 80 MeV/nucleon, meanwhile, the medium and breakup effects nearly cancel each other, so that only the non-BSS effect remains for Γ_{R}. Since the non-BSS effect is smaller at lower E_{in}, we can conclude that lower-incident energy scattering can be a good probe for evaluating Γ_{rds} from σ_{R}.

As mentioned above, the non-BSS effect becomes large as E_{in} increases. In the high-E_{in} region where the eikonal approximation is valid, σ_{R} is proportional to the volume integral of the imaginary part $\langle\varphi_0|W|\varphi_0\rangle$ of $\langle\varphi_0|U|\varphi_0\rangle$ [14,25], since

$$\sigma_{\mathrm{R}} = \int d^2\boldsymbol{b}[1 - |\langle\varphi_0|S|\varphi_0\rangle|^2] = \frac{-2}{\hbar v_0}\int d^3\boldsymbol{R}\langle\varphi_0|W|\varphi_0\rangle \tag{10}$$

with

$$S = \exp\left[-\frac{i}{\hbar v_0}\int_{-\infty}^{\infty} dZ U\right], \tag{11}$$

where v_0 is the incident velocity of P and $\boldsymbol{R} = (\boldsymbol{b}, Z)$. It follows from Eq. (10) that $\Gamma_{\mathrm{R}} = 0$.

Summary. The present microscopic version of three- and four-body CDCC calculations reproduces σ_{R} for $^{14,15,16}\mathrm{C} + {}^{12}\mathrm{C}$ scattering at 83 MeV/nucleon. The projectile-breakup effect is significant for $^{15}\mathrm{C}$ scattering and appreciable for $^{16}\mathrm{C}$ scattering, whereas the nuclear-medium effect is sizable for $^{14,15,16}\mathrm{C}$ scattering. In general, the σ_{R}-staggering Γ_{R} is deviated from the radius-staggering Γ_{rds} by the non-BSS, nuclear-medium, and projectile-breakup effects. At lower E_{in} from 50 to 80 MeV/nucleon, the breakup and medium effects nearly cancel and the remaining non-BSS effect is rather small for Γ_{R}. Therefore, the lower-E_{in} scattering can be a good probe for evaluating Γ_{rds} from σ_{R}. At high E_{in}, meanwhile, the non-BSS effect is significant, whereas the nuclear-medium and projectile-breakup effects are small or negligible. The non-BSS effect largely reduces Γ_{R} from Γ_{rds}. Thus the radius-staggering Γ_{rds} is masked by the non-BSS effect at high E_{in}. The present fully consistent microscopic calculations underestimate the experimental staggering $\Gamma_{\mathrm{R}}^{\mathrm{exp}} = 2.0 \pm 0.8$, though the calculated Γ_{R} clearly correlates with Γ_{rds}. In order to draw a definite conclusion on the pairing anti-halo effect, the reaction cross sections at low E_{in} should be further investigated both experimentally and theoretically.

Acknowledgments. The authors would like to thank M. Fukuda and T. Yamaguchi for helpful discussions. This work is supported in part by JSPS KAKENHI Grants No. 244137, No. 25·949, and No. 22540285.

[1] I. Tanihata *et al.*, Phys. Rev. Lett. **55**, 2676 (1985); Phys. Lett. B **206**, 592 (1988); I. Tanihata, J. Phys. G **22**, 157 (1996).
[2] A. Ozawa *et al.*, Nucl. Phys. A **691**, 599 (2001).
[3] M. Takechi *et al.*, Phys. Lett. B **707**, 357 (2012).
[4] K. Minomo *et al.*, Phys. Rev. C **84**, 034602 (2011).
[5] K. Minomo *et al.*, Phys. Rev. Lett. **108**, 052503 (2012).
[6] T. Sumi *et al.*, Phys. Rev. C **85**, 064613 (2012).
[7] K. Bennaceur *et al.*, Phys. Lett. B **496**, 154 (2000).
[8] K. Hagino and H. Sagawa, Phys. Rev. C **84**, 011303 (2011).
[9] K. Hagino and H. Sagawa, Phys. Rev. C **85**, 014303 (2012).
[10] K. Hagino and H. Sagawa, Phys. Rev. C **85**, 037604 (2012).
[11] D. Q. Fang *et al.*, Phys. Rev. C **69**, 034613 (2004).
[12] M. Kamimura *et al.*, Prog. Theor. Phys. Suppl. **89**, 1 (1986).
[13] N. Austern *et al.*, Phys. Rep. **154**, 125 (1987).
[14] M. Yahiro *et al.*, Prog. Theor. Exp. Phys. **2012**, 01A206 (2012).
[15] K. Amos *et al.*, in *Advances in Nuclear Physics*, edited by J. W. Negele and E. Vogt (Plenum, New York, 2000), Vol. 25, p. 275.
[16] H. de Vries *et al.*, At. Data Nucl. Data Tables **36**, 495 (1987).
[17] J. F. Berger *et al.*, Comput. Phys. Commun. **63**, 365 (1991).
[18] R. Machleidt, Adv. Nucl. Phys. **19**, 189 (1989).
[19] T. Matsumoto *et al.*, Phys. Rev. C **73**, 051602(R) (2006).
[20] L. A. Schaller *et al.*, Nucl. Phys. A **379**, 523 (1982).
[21] T. Matsumoto *et al.*, Phys. Rev. C **68**, 064607 (2003).
[22] T. Furumoto, W. Horiuchi, M. Takashina, Y. Yamamoto, and Y. Sakuragi, Phys. Rev. C **85**, 044607 (2012).
[23] R. A. D. Piyadasa *et al.*, Prog. Theor. Phys. **81**, 910 (1989).
[24] S. Hashimoto *et al.*, Phys. Rev. C **83**, 054617 (2011).
[25] M. Yahiro, M. Yahiro, K. Ogata, K. Minomo, and S. Chiba, Prog. Theor. Phys. **126**, 167 (2011).